Oxidation or Nitridation Behavior of Pure Chromium and Chromium Alloys Containing 10 mass%Ni or Fe in Atmospheric Heating

Oxidation or Nitridation Behavior of Pure Chromium and Chromium Alloys Containing 10 mass%Ni or Fe in Atmospheric Heating

Kaori Taneichi[1,*], Takayuki Narushima[2], Yasutaka Iguchi[1] and Chiaki Ouchi[1]

[1]*Department of Materials Processing, Tohoku University, Sendai 980-8579, Japan*
[2]*Tohoku University Biomedical Engineering Research Organization (TUBERO), Sendai 980-8579, Japan*

The oxidation or nitridation behavior of pure chromium and chromium alloys containing 10 mass%Ni or 10 mass%Fe in atmospheric heating was investigated in the temperature range of 1073 to 1373 K. The formation behavior of the outer oxide phase of Cr_2O_3 and its growth kinetics in both chromium alloys was very similar to that of pure chromium. The nitride layer with the Cr_2N phase was formed beneath the oxide phase at temperatures above 1273 K in pure chromium. Marked internal nitridation with the formation of the Cr_2N phase was observed in the Cr-10 mass%Fe alloy, while the formation of Cr_2N was negligible in the Cr-10 mass%Ni alloy. Neither Ni nor Fe were detected inside the Cr_2O_3 phase, and was enriched in the subsurface layer between the oxide layer and the base alloy in a respective alloy. The Ni-enriched layer in Cr-10 mass%Ni alloy had a relatively narrow width, but a very high concentration of Ni compared with the Fe-enriched layer formed in the Cr-10 mass%Fe alloy.   [doi:10.2320/matertrans.47.2540]

1. Introduction

Chromium is one of the metals with a high melting point similar to Mo or W, and it has excellent high temperature creep properties as well as very high corrosion resistance properties in various corrosive environments.[1–3] It is also widely utilized as an alloying element in stainless steels and Ni-base alloys because the protective surface film of Cr_2O_3 formed in various environments improves the corrosion resistance of these alloys. Nevertheless, pure chromium and chromium-based alloys have never become engineering materials for structural use because of their brittleness or extremely poor ductility at both ambient and elevated temperatures.

However, it was made clear that chromium was not intrinsically brittle, but rather it was brought about from impurities such as nitrogen, oxygen, sulfur or carbon in chromium.[3] That is, high purification of chromium or scavenging of impurities by adding micro alloying elements could improve workability and reduce the ductile-brittle transition temperature of chromium.[3,4] Recently, high purification processes for chromium such as electro-refining in chromium acid salt or iodide have been developed, which had been studied originally in the 1950s.[5–7] In addition, manufacturing of wrought chromium was enabled by development of the powder metallurgy process and the pack rolling process.[8–11] These current progresses have stimulated practical uses of highly pure chromium and chromium alloys as a wrought material for structural use in addition to its use as a sputtering target material.

For industrialization of wrought pure chromium or chromium alloys, it is very important to study details of oxidation or nitridation behavior of these materials which take place during atmospheric heating in hot working or heat treatment. Early oxidation studies of chromium had been performed from the 1950s to the beginning of the 1970s, and several studies on high temperature oxidation or nitridation behavior of chromium under a pure oxygen or nitrogen gas atmosphere had been reported.[12–19] Lillerud and Kofstad summarized the past oxidation kinetics studies of pure chromium, and discussed in detail the causes for the large variation in parabolic rate constant values reported in numerous past studies.[20,21] However, very few studies of oxidation and nitridation of chromium-based alloys in atmospheric heating have been carried out,[16,22] and no detailed analyses of scale and subsurface regions have yet been reported.

It is important to study in greater detail the oxidation and nitridation behavior in pure chromium and, in particular, chromium-based alloys under atmospheric heating condition, because the surface or internal oxidation and nitridation data obtained in conjunction with heating variables such as the heating temperature or heating time period can be used to determine or optimize the heating conditions in hot working or heat treatment for chromium materials. Therefore, the present study was conducted to investigate oxidation and nitridation behavior under atmospheric heating condition in pure chromium with purity of 99.99% and chromium alloys containing 10 mass%Ni or 10 mass%Fe. The growth rate of the oxidation layer was measured and the rate constant is discussed as well as identification of various phases formed on the surface and subsurface of pure chromium and these two chromium alloys. In the chromium alloys, we focused on the effect of the Ni- or Fe-enriched layer formed beneath the outer oxide layer on oxidation or nitridation behavior in the respective alloy.

2. Experimental Procedures

The pure chromium and chromium alloys used in this study were prepared using an argon arc melting furnace with

---

*Graduate Student, Tohoku University. Present address: Japan Air line Co., Ltd., Narita 282-8610, Japan

Table 1   Chemical composition of pure chromium and chromium alloys.

Materials	Composition/mass%			
	O	N	Ni	Fe
Pure chromium	0.0259	0.0004	—	—
Cr-10 mass%Ni	0.0381	0.0113	9.81	—
Cr-10 mass%Fe	0.0377	0.0006	—	9.98

a non-consumable tungsten electrode. The raw materials used for melting were 99.99% purity chromium with a flake shape, 99.99% purity Ni granules and 99.9% purity Fe granules. The granular size of Ni and Fe was 3 to 10 mm and 5 to 10 mm in diameter, respectively. The size of button ingots prepared was 15 mm in thickness and 40 mm in diameter. The chemical composition of these button ingots is shown in Table 1. Hereafter, the Cr-10 mass%Ni and Cr-10 mass%Fe alloys are noted as Cr-10Ni and Cr-10Fe alloys, respectively. The oxygen contents in these materials were between 0.025 and 0.038 mass% and nitrogen contents were less than 0.001 mass% except for Cr-10Ni alloy, in which the nitrogen content was much higher than that in other materials. The cause for this increase in nitrogen content was not clear.

The button ingot of pure chromium was isothermally hot-forged from 15 to 6.1 mm thickness at 1373 K. The hot forged plate was machined to a 2 mm thick sheet. The button ingots of chromium alloys were homogenized at 1373 K, and were directly machined to 2 mm thick sheets without forging. Sheet surface was polished using emery papers up to #2000 and buff polished with alumina powder of 0.3 μm in diameter. The dimensions and mass of the specimens were measured, followed by cleaning ultrasonically in acetone.

Atmospheric heating experiments were conducted using a box type furnace with electric resistant heating elements. The box type furnace was heated to the specified temperature at heating rate of 5.56×10^{-2} K·s^{-1}. After the temperature of the furnace was stabilized, the specimens put on a silica dish were inserted into the furnace to initiate the heating experiment. The heating temperature range was between 1073 and 1373 K, and the heating time periods at a constant temperature were varied from 3.6 to 36 ks. After heating for a specified time period, the specimens were pulled out from the furnace together with the dish, followed by air cooling. The mass gain of the heated specimens due to oxidation or nitridation was defined by the difference in mass between as-polished and heated specimens. The thickness of the oxide layer was also metallographically measured by cross-sectional observation. The observation and identification of the phases formed on the surface or subsurface of the heated specimens were performed by SEM/EDX (S-3100H, Hitachi), XRD (X' Pert, PHILIPS) and EPMA (EPMA-8750, Shimadzu).

3.   Results

3.1   Oxidation kinetics

Figure 1 shows the mass change of pure chromium with the heating time in air. The solid lines at a respective temperature shown in the figure were drawn by assuming a parabolic rate law except the line at 1373 K. Almost all data
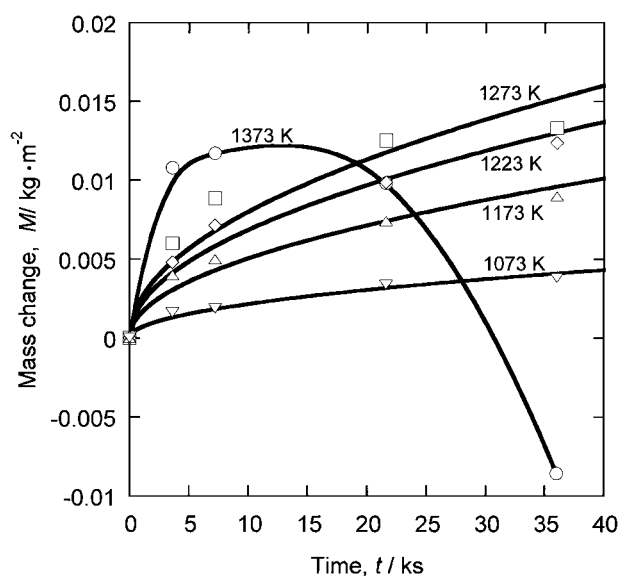

Fig. 1   Mass change of pure chromium with heating time in air.

are well fitted to these lines in the temperature range of 1073 to 1273 K. The severe spalling or cracking of the outer oxide layer took place with increased heating time at 1373 K, making the exact measurement of mass gain difficult. Adhesion of the oxide layer to the base metal was first lost in the heating time period of 36 ks at 1223 K. Local detachment at the interface between the oxide phase and the base metal was observed at a much shorter heating time at 1273 K. The increase in the oxide layer thickness enhanced the detachment at the interface. The results of mass gain variations with the heating temperature and the heating time in Cr-10Ni and Cr-10Fe alloys were very similar to those of pure chromium.

As described later, the nitridation layer with Cr$_2$N phase was formed beneath the outer oxide layer in pure chromium at high temperatures, and marked internal nitridation took place in Cr-10Fe alloy. Therefore, the oxidation rates of chromium materials cannot be evaluated by measurement of the mass gain, and the thickness change of the oxidized layer with the heating time was measured in pure chromium and both chromium alloys as shown in Figs. 2 to 4. The oxide layer thickness of the specimens heated at 1373 K was measured using the oxide layer which remained partially on the surface without detachment. Solid lines for various temperatures in Figs. 2 to 4 were drawn by assuming a parabolic rate law similar to Fig. 1, and it is found that the most of the data well coincide with these lines. Actually, the gradient in log-log plots for oxide thickness and heating time were 0.4–0.6 for pure chromium and Cr-10Fe, and 0.3–0.8 for Cr-10Ni. That is, growth of the oxide phase is controlled by the parabolic rate law in pure chromium and both chromium alloys.

The parabolic rate constants and activation energy in pure chromium and chromium alloys for oxidation obtained from the results shown in Figs. 2 to 4 are summarized in Table 2. The values of activation energies in pure chromium and Cr-10Ni alloy shown in Table 2 are largely changed at the temperatures of 1223 and 1273 K, respectively, which
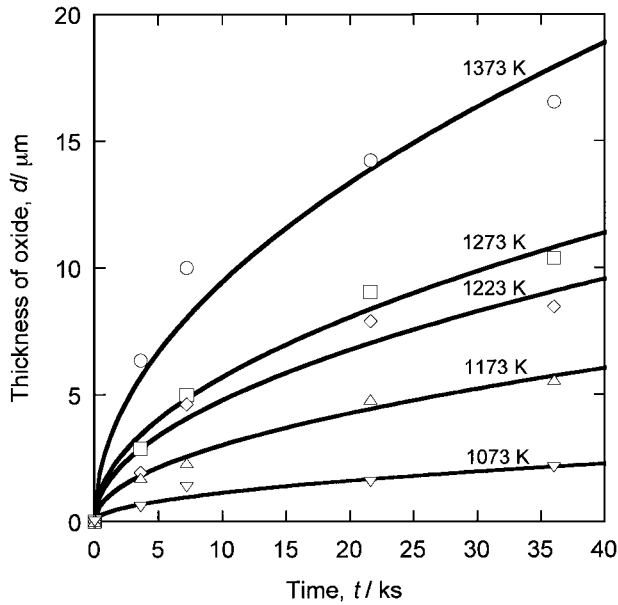
Fig. 2 Changes in the oxide thickness of pure chromium with heating time in air.
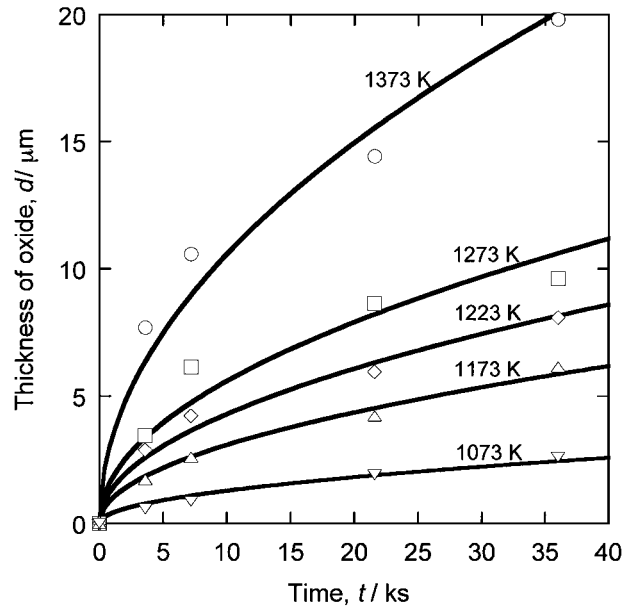

Fig. 4 Changes in the oxide thickness of Cr-10 mass%Fe alloy with heating time in air.
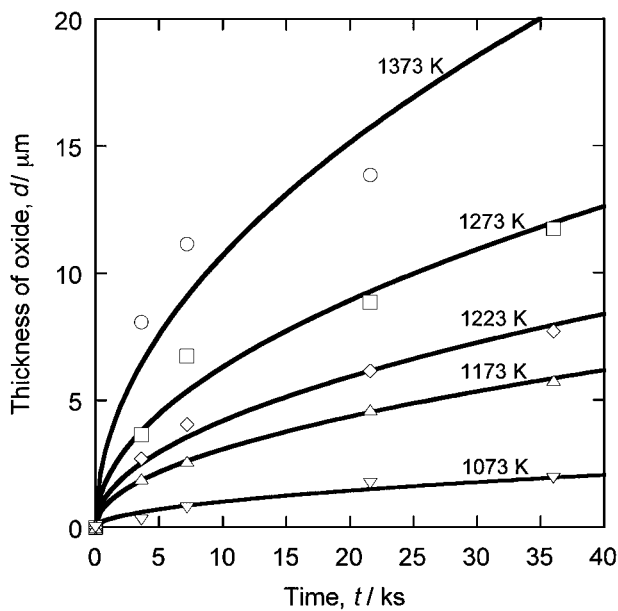

Fig. 3 Changes in the oxide thickness of Cr-10 mass%Ni alloy with heating time in air.

will be discussed in the next section. Below these temperatures, the values of parabolic rate constants of pure chromium are almost the same as those of Cr-10Ni alloy and larger than that of Cr-10Fe alloy, and above these temperatures activation energy values in pure chromium and Cr-10Ni alloy decrease.

3.2 Microstructural observations of surface layer and subsurface region

The surface layer and the subsurface region in the cross-section of the specimens in pure chromium and in Cr-10Ni and Cr-10Fe alloys were observed by scanning electron microscopy (SEM). The examples for the specimens heated at 1273 K for 36 ks are shown in Fig. 5. The two phases are formed in pure chromium, and the outer and inner layers were confirmed to be the oxide phase of Cr_2O_3 and the nitride phase of Cr_2N, respectively, by XRD and EPMA. The Cr_2N phase is first formed in a lens-like shape discontinuously along the interface between the Cr_2O_3 phase and the base metal as seen in Fig. 6(a), of which specimen was heated at the temperature of 1273 K for 21.6 ks. A fairly thick layer of the nitride phase with almost the same thickness of the outer oxide layer is uniformly formed at the temperature of 1373 K for 36 ks as seen in Fig. 6(b), where the oxide layer was no longer observed as an outer layer due to its severe spalling. The nitride formation was not observed at temperatures below 1173 K except at the specimen edges. The quantitative measurement of the nitride layer thickness was not performed

Table 2 Parabolic rate constants (k_p) and activation energies (E) for oxidation of pure chromium and chromium alloys.

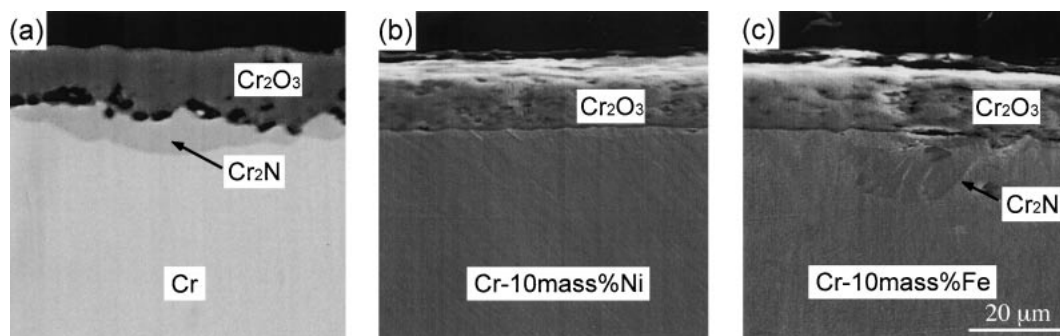|	Temp./K	Pure chromium	Cr-10 mass%Ni	Cr-10 mass%Fe
$k_p/m^2 \cdot s^{-1}$	1073	1.24×10^{-16}	1.11×10^{-16}	1.80×10^{-16}
	1173	9.14×10^{-16}	9.42×10^{-16}	9.89×10^{-16}
	1223	2.24×10^{-15}	1.69×10^{-15}	1.79×10^{-15}
	1273	3.20×10^{-15}	3.84×10^{-15}	2.88×10^{-15}
	1373	8.26×10^{-15}	9.92×10^{-15}	1.07×10^{-14}
$E/kJ \cdot mol^{-1}$		210 (1073–1223 K)	200 (1073–1273 K)	164 (1073–1373 K)
		124 (1223–1373 K)	138 (1273–1373 K)	

Fig. 5　Cross-sectional observations of the surface layer and the subsurface region of specimens heated at 1273 K for 36 ks by SEM, (a) pure chromium, (b) Cr-10 mass%Ni and (c) Cr-10 mass%Fe.
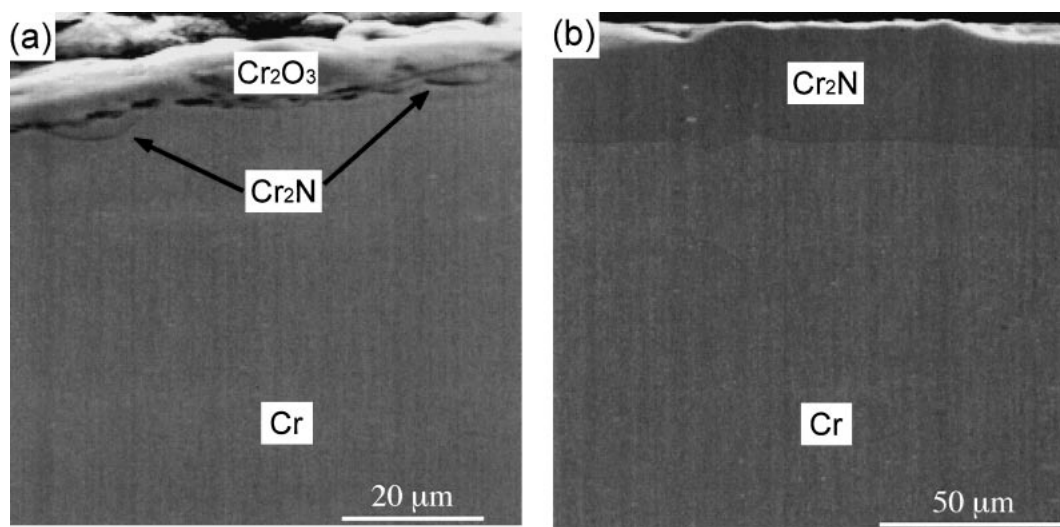

Fig. 6　Cross-sectional observations of the surface layers of pure chromium by SEM, heated at (a) 1273 K for 21.6 ks and (b) 1373 K for 36 ks.

because uniformity and morphology of the nitride phase varied widely depending on the heating temperature. The formation of the numerous voids is observed near the interface between Cr_2O_3 and Cr_2N or the metal matrix and also at the inside of the Cr_2O_3 phase as shown in Figs. 5 and 6.

Only the Cr_2O_3 phase was formed in both chromium alloys, with no formation of the nitride layer beneath the Cr_2O_3 phase as observed in pure chromium. It was confirmed by EPMA that neither Ni nor Fe were contained in the oxide phase of either chromium alloy, and that these alloying elements were enriched at the interface between the oxide phase and the base alloy. The examples of the cross-sectional analysis of Ni or Fe concentration in the enriched phase of both alloys are exhibited in Fig. 7, where the specimens were heated at 1273 K for 21.6 ks. The width of the Ni-enriched layer is 1.8 μm, which is much thinner than that of Fe-enriched layer, 4 μm. The maximum Ni and Fe concentrations in the enriched layer formed under this heating condition are 50 and 30 mass%, respectively. In other heating conditions, the Ni concentration was always higher than the Fe concentration.

The nitride phase with an island shape formed in the alloy matrix seen in Fig. 5(c) was caused by internal nitridation.

Marked internal nitridation was observed only in Cr-10Fe alloy. The internal nitridation was not detected in pure chromium or Cr-10Ni alloy, although a very small amount of Cr_2N was detected in the latter alloy by XRD analysis in the specimens heated at temperatures above 1273 K, but was not detected by SEM/EDX. The phase of this internal nitridation in Cr-10Fe alloy was confirmed to be Cr_2N by XDR and EPMA. The distribution of various elements in the subsurface area of cross-section in Cr-10Fe alloy was analyzed by SEM/EDX as shown in Fig. 8, where the specimen was heated at 1273 K for 21.6 ks. The existence of the oxide layer, the Fe-enriched phase and internal nitridation in the alloy matrix are clearly shown by the composition images of Fe, O and N.

As seen in Fig. 5, many voids were formed near the interface and in the oxide phase in pure chromium while the voids were detected in the oxide phase formed in chromium alloys. The numerous wrinkles or the wavy pattern on the surface of the oxide layer were observed after the specimens were cooled. This seemed to be formed during cooling due to differences in the thermal expansion coefficient between Cr and Cr_2O_3 or Cr_2N. The thermal expansion coefficients of Cr_2O_3, Cr and Cr_2N are 7.3, 9.5 and 9.41×10^{-6}, respectively. Kofstad and Lillerud[21] reported that this wavy
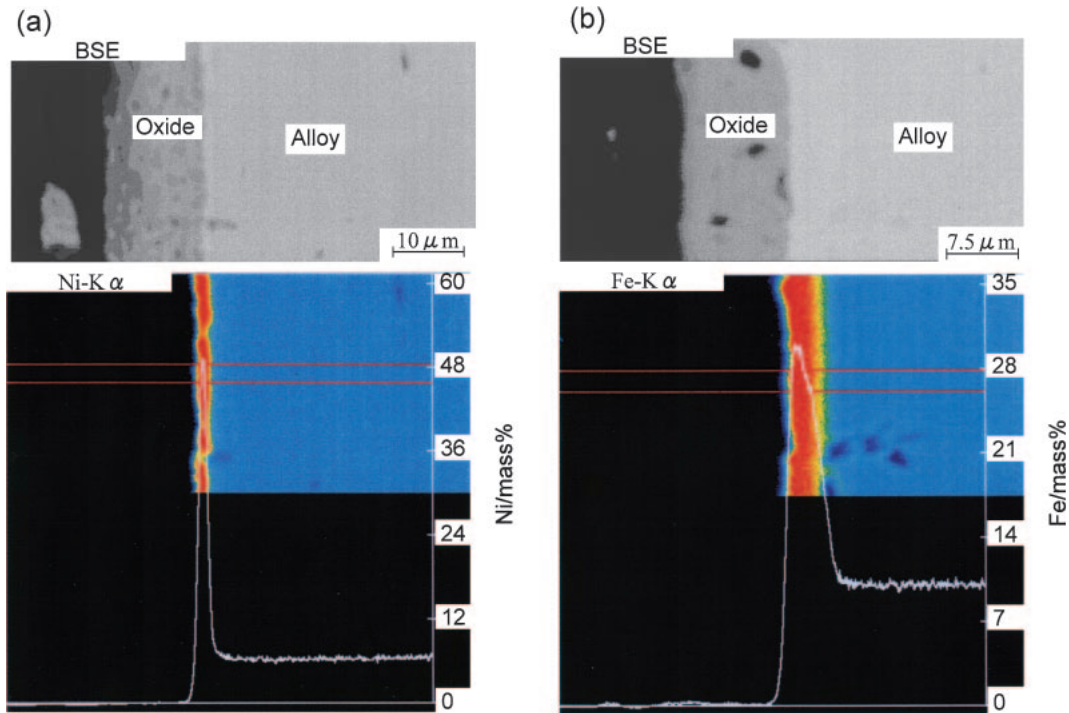
Fig. 7 Cross-sectional analysis of Ni and Fe concentrations in Ni- and Fe-enriched phases formed below the oxide layer in (a) Cr-10 mass%Ni and (b) Cr-10 mass%Fe alloys, respectively. The specimens were heated at 1273 K for 21.6 ks.
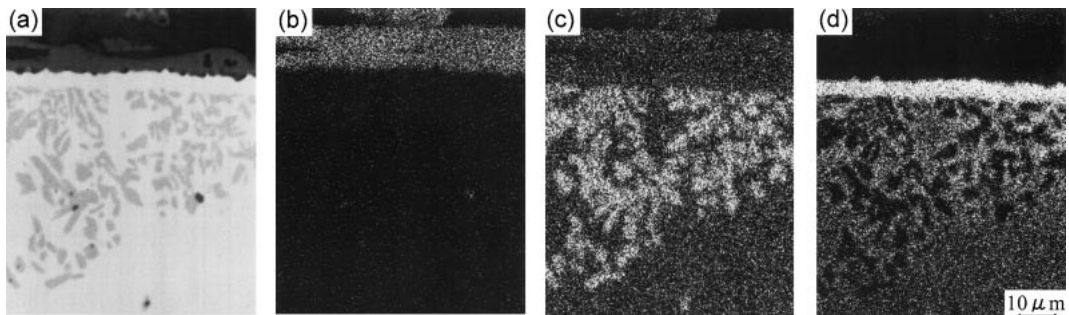

Fig. 8 SEM/EDX analysis of the surface and the subsurface region in cross-section of specimens heated at 1273 K for 21.6 ks in Cr-10 mass%Fe alloy, (a) back-scattered electron image, and Kα images of (b) O, (c) N and (d) Fe.

appearance was due to buckles in the oxide phase caused by deformation due to compressive stress in the oxide phase.

4. Discussion

The past studies of the oxidation kinetics of pure chromium were mostly conducted in pure oxygen atmosphere under the control of partial pressure,[12,14,17,19,20] and the parabolic rate growth of Cr_2O_3 was realized in the temperature range of 1023 to 1373 K, while the effect of partial pressure of oxygen on the parabolic rate constant value was relatively small. The growth of the Cr_2O_3 layer seems to be controlled by diffusion of the Cr cation through the Cr_2O_3 layer because the voids were observed beneath the outer Cr_2O_3 layer. Actually, it was reported that the cation was much more mobile in Cr_2O_3 than was the anion.[23]

The temperature dependence of k_p values of chromium obtained in oxygen or in air atmosphere is shown in Fig. 9, comparing the present results with those reported by other

groups. The values of k_p obtained by mass gain measurements were converted into k_p values by thickness measurement of Cr_2O_3 layer, assuming that all the mass gain was due to the formation of the Cr_2O_3 layer. All other k_p values except the present study were obtained by a thermogravimetric method. Lillerud and Kofstad summarized parabolic rate constants (k_p) reported by many research groups, finding that k_p values varied by more than four orders of magnitude in the temperature range of 1273 to 1473 K.[20,21] The cause of a large discrepancy in k_p values was discussed based on differences in specimen surface preparation methods, reaction conditions or purity of chromium. The present result is located in the upper side of a wide band of k_p values. It is not easy to determine which one among various possible causes of the large discrepancy described above is the strongest factor. However, it is important to note here that Cr_2N phase beneath the outer Cr_2O_3 phase was formed at temperatures above 1273 K by atmospheric heating in the present study. The formation of a nitride layer in pure chromium seems to
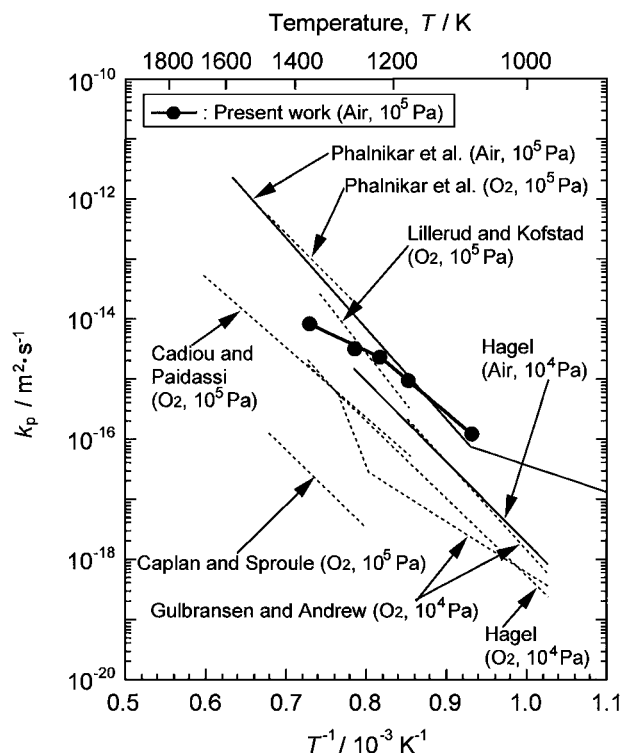
Fig. 9 Comparison of temperature dependence of parabolic rate constant values (k_p) for oxidation of pure chromium among the present and other reported results.

result in reduction of k_p values and activation energy in the higher temperature region, because the existence of a chromium nitride phase retarded Cr supply from the base metal. As for Cr-10Ni alloy, the formation of an Ni-enriched layer with high Ni concentration may decrease k_p values. The width of the Ni-enriched layer is much thinner than that of the Fe-enriched layer, and the maximum Ni concentration in the enriched layer was higher than the maximum Fe concentration. These results suggest that the diffusion coefficient of nickel in chromium may be smaller than that of iron, although the available diffusion coefficient of nickel in chromium was not found in the literature.

The discontinuous formation of Cr_2N phase along the interface between Cr_2O_3 phase and the base metal started from the temperatures around 1273 K in pure chromium. It had been well confirmed that the detachment between Cr_2O_3 and the base metal took place in this temperature region, forming discontinuous cavities at the interface. The partial pressure of oxygen at this interface corresponds to the decomposition pressure of Cr_2O_3 in equilibrium with chromium metal, being around 10^{-17} Pa at 1273 K,[24] and such a low oxygen pressure in cavities may be favorable for the formation of a Cr_2N phase in combination of high vapor pressure of chromium. Nitrogen atoms may diffuse from the outer surface through oxide by grain boundary or bulk diffusion, forming nitride at the interface. This nitride phase was formed very uniformly by heating at 1373 K as shown in Fig. 6(b). This seems to be due to forming of continuous detachment at the interface. The growth rate of nitride may be controlled by nitrogen diffusion through the oxide phase. In the chromium alloys, however, no continuous nitride layer

was observed. The Fe- and Ni-enriched layers lowered the vapor pressure of chromium in the cavity and prevented the formation of the continuous nitride layer. The internal nitridation was detected in Cr-10Fe alloy. Nitrogen diffuses through the outer oxide layer and the Fe-enriched layer and reacts with chromium to form Cr_2N, while no internal nitridation was detected in pure chromium or Cr-10Ni alloy. The diffusion coefficient of nitrogen in nickel at temperatures lower than 773 K was reported, and the value of nitrogen diffusion coefficient at the temperature of 1273 K extrapolated from this data was 4×10^{-14} m^2·s^{-1}, which is much smaller than that in iron or chromium.[25] These analyses based on diffusion coefficients suggest that the Ni-enriched layer may act as a barrier against nitrogen diffusion and that the nitrogen transport is not enough to form the nitride beneath the Ni-enriched layer.

It was reported in a high-temperature nitridation study of chromium in nitrogen atmosphere that CrN and Cr_2N were formed[15] and that the value of parabolic rate constant in nitridation was larger than that in oxidation.[16] Kodentsov et al.[26] studied nitridation of Ni-Cr alloys under a wide range of pure nitrogen gas pressure from 10^5 Pa to 6×10^8 Pa. At high nitrogen pressures, the formation of the outer surface layer was the CrN phase, and the internal nitridation was CrN for Cr content below 22 at% in Ni-Cr alloy and Cr_2N for Cr content over 28 at%. At 10^5 Pa, the Cr_2N phase was formed in the outer surface layer and also the internal precipitates in the alloy containing Cr over 28 at%. The main nitride phase formed in the present study was the Cr_2N phase because of the lower nitrogen pressure and higher chromium contents.

No nickel or iron oxide was found in the oxide phase in chromium alloys because of higher oxygen affinity of chromium than that of Ni or Fe. The selective oxidation of chromium yielded the formation of an Ni- or Fe-enriched alloy phase beneath the outer oxide layer.

5. Conclusions

The oxidation or nitridation behavior of pure chromium and chromium alloys containing 10 mass%Ni or 10 mass%Fe during atmospheric heating was investigated in the temperature range of 1073 to 1373 K. The main results obtained are summarized as follows.

(1) The changes of oxide layer thickness with heating time in pure chromium and both chromium alloys were controlled by a parabolic rate law, and the rate controlling process for oxidation was Cr cation diffusion through the outer Cr_2O_3 oxide layer.

(2) The nitride phase of Cr_2N was formed beneath the outer oxide layer of Cr_2O_3 in pure chromium. However, no nitride layer beneath the oxide phase was detected in either chromium alloy.

(3) The Ni-enriched and Fe-enriched layers were formed beneath the outer oxide layer in Cr-10 mass%Ni and Cr-10 mass%Fe alloy, respectively. The former thickness was much thinner than the latter, corresponding to the results that the maximum Ni concentration in the Ni-enriched layer was much higher than the maximum Fe concentration in Fe-enriched layer.

(4) The marked internal nitridation with forming Cr_2N

below the Fe-enriched layer was observed in Cr-10 mass%Fe alloy, but was not detected in pure chromium and Cr-10 mass%Ni alloy. The Ni-enriched layer with very high Ni concentration appeared to prevent internal nitridation.

REFERENCES

1) R. Eck, H. P. Martinz, T. Sakaki and M. Kato: Mater. Sci. Eng. A **120** (1989) 307–312.
2) M. Yoshiba, H. Wada, T. Sakaki and M. Kato: J. Jpn. Inst. Metals **54** (1990) 794–801.
3) T. Sakaki: J. High Temp. Soc. **18** (1992) 157–163.
4) Y. Oba: Bull. Jpn. Inst. Metals **11** (1972) 105–112.
5) H. T. Greenaway: J. Inst. Metals **83** (1954-55) 121–125.
6) F. Henderson, S. T. Quaass and H. L. Wain: J. Inst. Metals **83** (1954-55) 126–132.
7) D. J. Maykuth, W. D. Klopp, R. I. Jaffee and H. B. Goodwin: J. Electrochem. Soc. **102** (1955) 316–331.
8) M. Ohmori, A. Kaya, Y. Harada, F. Yoshida and M. Itoh: J. Jpn. Inst. Metals **52** (1988) 223–228.
9) Y. Harada, M. Ohmori, F. Yoshida and M. Itoh: J. Jpn. Inst. Metals **53** (1989) 201–205.
10) Y. Harada, M. Ohmori, F. Yoshida and M. Itoh: J. Jpn. Inst. Metals **53** (1989) 921–926.
11) H. Harada, M. Ohmori and S. Ohnishi: J. Jpn. Inst. Metals **54** (1990) 473–479.
12) E. A. Gulbransen and K. F. Andrew: J. Electrochem. Soc. **99** (1952) 402–406.
13) C. A. Phalnikar, E. B. Evans and W. M. Baldwin, Jr.: J. Electrochem. Soc. **103** (1952) 429–438.
14) E. A. Gulbransen and K. F. Andrew: J. Eletrochem. Soc. **104** (1957) 334–338.
15) T. Miyakawa and S. Okamoto: J. Jpn. Inst. Metals **23** (1959) 568–572.
16) W. C. Hagel: A.S.M. Trans. Quarterly **56** (1963) 583–599.
17) L. Cadiou and J. Paidassi: Mem. Sci. Rev. Metall. **66** (1969) 217–225.
18) J. L. Arnold and W. C. Hagel: Metall. Trans. **3** (1972) 1471–1477.
19) D. Caplan and G. I. Sproule: Oxi. Met. **9** (1975) 459–472.
20) K. P. Lillerud and P. Kofstad: J. Electrochem. Soc. **127** (1980) 2397–2409.
21) P. Kofstad and K. P. Lillerud: J. Electrochem. Soc. **127** (1980) 2410–2419.
22) O. Kubaschewski and A. Schneider: J. Inst. Metals **75** (1949) 403–416.
23) W. C. Hagel and A. U. Seybolt: J. Electrochem. Soc. **108** (1961) 1146–1152.
24) *NIST-JANAF Thermochemical Tables*, Fourth Ed., ed by M. W. Chase, Jr., (ACS and AIP for NIST, 1998).
25) *Landolt-Börnstein Numerical data and functional relationships in science and technology*, Crystals and solid state physics, Volume 26 Diffusion in solid metals and alloys, Berlin, (Springer-Verlag, 1990).
26) A. A. Kodentsov, J. H. Gülpen, C. Cserháti, J. K. Kivilahti and F. J. J. van Loo: Metall. Mater. Trans. A **27A** (1996) 59–69.